FIVE MARTIAN YEARS OF MSL GALE CRATER CLOUD OPACITY MEASUREMENTS: DETERMINING A SCATTERING PHASE FUNCTION FOR THE APHELION CLOUD BELT

C. W. Hayes[1] *(hayes954@yorku.ca)*, **J. L. Kloos[2], C. L. Campbell[1], A. C. Innanen[1], H. M. Sapers[1], and J. E. Moores[1].** *[1]Centre for Research in Earth and Space Sciences, York University, Toronto, ON, Canada; [2]Department of Astronomy, University of Maryland, College Park, MD, USA.*

Introduction:

The Martian climate is dominated by the seasonal effects of the planet's high orbital eccentricity (~0.0935), which takes it ~20% closer to the Sun at perihelion than at aphelion. This difference results in significant variations in solar insolation and thus atmospheric conditions over the course of the Martian year. Two Martian seasons can thus be defined: the dusty season, which occurs around perihelion (L_s = 135° - 360°) and is characterized by higher temperatures and increased atmospheric dust loading; and the cloudy season, which occurs around aphelion (L_s = 0° - 135°) and is characterized by the formation of the Aphelion Cloud Belt (ACB), a water-ice cloud feature that surrounds the planet at latitudes between 10°S and 30°N (Wolff et al., 1999).

Although the thickness of the ACB peaks around 10°N, the equatorial latitude of the Mars Science Laboratory (MSL) Curiosity rover landing site (~4.6°S) allows for observations of the southern edge of the ACB to be conducted from the ground. With this in mind, a cloud observation campaign has been ongoing since sol 24 with the goal of examining diurnal, annual, and interannual variations in cloud opacities, morphologies, and altitudes, as well as their scattering phase function.

Previous work (Moores et al., 2015; Kloos et al., 2016; Kloos et al., 2018) examined the first two Martian years of data and found a slight increase in opacities in the early morning compared to the late afternoon, as well as increased opacities overall during the ACB season. Kloos et al. (2018) also found very little interannual variability in the opacity of ACB clouds between MY 32 and MY 33, which is consistent with orbital observations of the interannual consistency of the ACB (e.g. Tamppari et al., 2003; Liu et al., 2003; Smith et al., 2004; Hale et al., 2011). Although an apparent increase in opacity in MY 33 is observed, it is attributed to an increased number of early morning observations, which pulled the average up on account of their higher opacities compared to afternoon clouds.

However, because consistent early morning observations were not conducted until MY 33, it was not possible for Kloos et al. (2018) to determine if the diurnal difference in opacity was a persistent or transient feature of the ACB. With five MYs of data processed, three and a half of which include full diurnal coverage, we can now fully assess the year-to-year variability of ACB clouds over Gale Crater.

Methods:

Atmospheric movies. Using the Navigation Cameras (Navcams) onboard MSL, two types of atmospheric movies are acquired on a regular cadence: Zenith Movies (ZMs) and Suprahorizon Movies (SHMs). ZMs are pointed almost directly straight up (~85°), allowing for the determination of the clouds' angular velocities and direction of motion; SHMs are pointed more obliquely (~26°), permitting a more robust examination of cloud morphologies. Both movies consist of eight frames taken across ~6 minutes.

On average, ZMs are acquired at a reduced cadence compared to SHMs because MSL's equatorial location mandates a two and a half hour keepout time from local noon to avoid pointing the Navcams directly at the Sun.

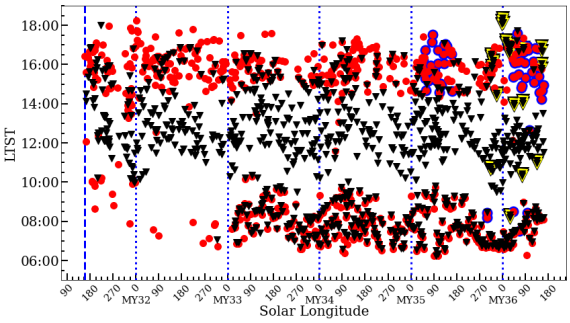

Figure 1. Temporal distribution of ZMs (red circles) and SHMs (black triangles) over the length of the MSL mission. The ZM keepout window is evident, as well as the addition of dedicated observation time in the morning be-ginning in MY33. The highlighted observations are CAO ZMs and SPENDIs/Super-SPENDIs, illustrating how the addition of these observations enhanced the cadence of opacity measurements. The gap in coverage around 10:00 LTST is the result of the rover's uplink schedule, which precludes observations.

In recent MYs, several new observations have been introduced that have allowed for an increased cadence of both ZMs and SHMs. First is the Cloud Altitude Observation (CAO; Campbell et al. 2020), which is executed ~once a week between 14:30–16:00 LTST during the ACB season. Though its primary purpose is to measure cloud altitudes, it includes a ZM that is identical to the standard cadence ZMs. The second new observation is a shunt prevention activity, designed to partially drain the rover's battery to prevent it from sitting fully-charged for an extended period of time. Two versions of this activity were designed, with low (SPENDI; Shunt Prevention ENV Navcam Drop-In) or high (Super-SPENDI) data

volumes to meet the rover's operational needs at different times of the year. Both versions consist of movies taken at six different pointings, two of which replicate the SHM parameters. They are not subject to the typical science block time limitations, and so have allowed for the acquisition of SHMs at atypical times of day, improving the diurnal coverage.

Opacity measurement. Martian clouds are typically very optically thin, so much so that they are rarely visible in the raw movie frames. Consequently, a technique known as mean-frame subtraction is used to enhance the visibility of clouds in each movie. Each pixel is averaged across all eight frames of the movie to produce a mean frame, which is then subtracted from each individual frame, leaving behind only the time-varying portion of the image (i.e., the clouds).

Figure 2. One frame from a SHM taken on sol 1924 before (left) and after (right) mean-frame subtraction, showcasing the ability of this method to extract the optically thin clouds from the background.

Following mean-frame subtraction, high- and low-radiance points, corresponding to a cloudy and non-cloudy portion of the image, respectively, are chosen from one frame through visual inspection. The difference in radiance between these two points ($I_{\lambda,VAR}$) is then used to determine the cloud opacity.

Opacities are calculated using two equations that make different assumptions about the nature of the clouds being observed, assumptions that are valid at different points during the year. The first of these equations, the *high-cloud* formula (Eq. 1), is used during the ACB season. It assumes that the clouds are at high altitudes and primarily comprised of water ice crystals. The second, the *whole atmosphere* formula (Eq. 2), assumes that MSL is observing low-altitude dust clouds. Opacities are found using both methods, then one is selected as the preferred opacity depending on whether equatorial water ice clouds are observed by the Mars Color Imager onboard the Mars Reconnaissance Orbiter at the time the movie was taken. For full derivations of these equations, see Kloos et al. (2016) and Moores et al. (2010).

$$\Delta\tau_{HC} = \frac{4\pi\mu I_{\lambda,VAR}\Delta\lambda}{P(\Theta)F_{\lambda,0}\,exp\left(-\frac{\tau_{COL}}{\mu}\right)} \quad (1)$$

$$\Delta\tau_{WA} = -ln\left[1 + a - \frac{a}{exp(-\tau_{COL})}\right] \quad (2)$$

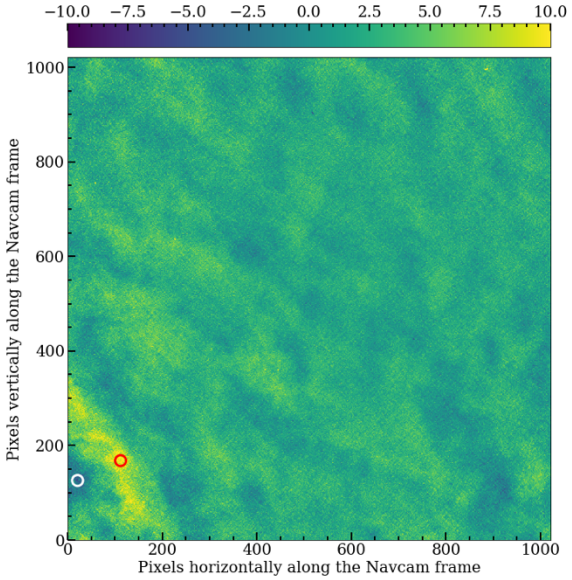

Figure 3. An example radiance map of the time-variable component of frame 5 of the sol 2633 ZM. The high and low radiance points are indicated by the red and white markers, respectively.

Working through these equations term by term, μ is the cosine of the zenith angle (5° for ZMs, 64° for SHMs), $I_{\lambda,VAR}$ is the difference in radiance between the selected high and low points, and Δλ is the Navcam bandpass (250 nm). P(Θ) is the scattering phase function of the clouds, $F_{\lambda,0}$ is the in-band solar flux at the top of the atmosphere, and τ_{COL} is the atmospheric column density, determined through Mastcam imaging of the solar disc every 5-10 sols (Lemmon, 2014). Finally, a is the fractional radiance, or the ratio of $I_{\lambda,VAR}$ and the mean radiance of the frame ($a = I_{\lambda,VAR}/I_{\lambda,MEAN}$).

Most of these terms are fairly well-determined. The two that introduce the most uncertainty into the opacity measurements are τ_{COL} and P(Θ). Because τ_{COL} is not acquired simultaneously (or even always on the same sol) as the cloud movies, it is necessary to interpolate between sols where τ_{COL} is measured. Though a linear interpolation is generally a good fit (Kloos et al., 2018), brief jumps in optical depth over short timescales have been measured near perihelion by the UV sensors on the Rover Environmental Monitoring Station. If such an increase occurred while a cloud observation was underway, a linear interpolation would be inappropriate.

P(Θ) is assumed to be independent of scattering angle, at a value of $P = 1/15$, or the ratio between the radiance and extinction coefficients for isotropic single scattering, the dominant form of radiative transfer given the low opacities of the clouds. This value is also consistent with measured cloud phase functions in the vicinity of 90°, where most of the cloud movies taken during MY 31–33 were acquired. Complementary observations of the phase function of Martian clouds from MSL that are currently ongoing (Cooper

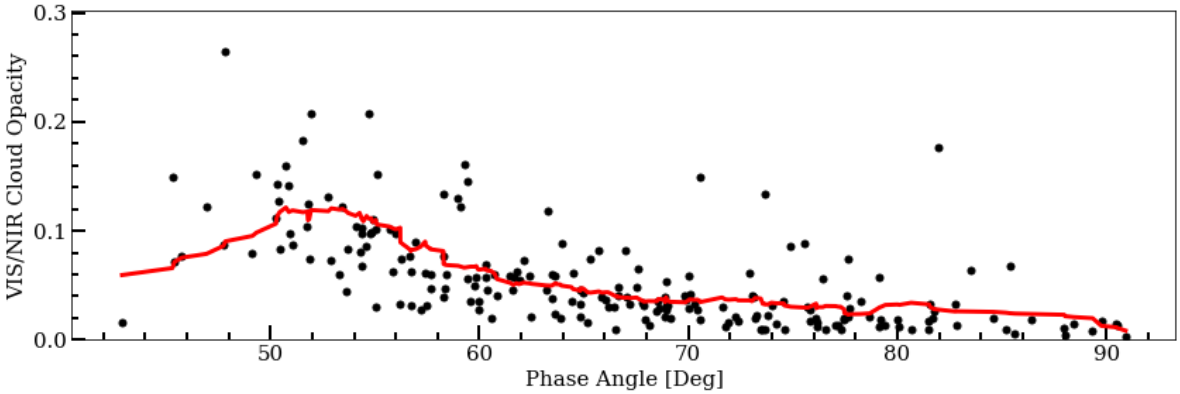

Figure 4. ZM cloud opacities as a function of phase angle. Note that these angles are measured with respect to the center of the Navcam frame, and not the points where the opacity was measured. These two angles can be ±30° from each other due to the wide FOV of the Navcams (45°). The red line is a moving average calculated with a window width of 25.

et al., 2019; Innanen et al. 2021) may lead to improved precision in this term in the future.

Results:

With all movies acquired through Ls = 160° of MY 36 processed, the record of cloud opacity measurements over Gale Crater has been extended from two Martian years to five. Notably, we now have ~3.5 MY of full AM/PM coverage, allowing us to examine interannual variability in diurnal opacity patterns for the first time.

Observations at low phase angles. During our preliminary analysis of movies acquired during MY 34–36, we discovered that the ZM and SHM datasets were producing different results for the preferred mean opacity during the ACB season. In theory, there is no good reason why the clouds observed in a SHM would be any different than those observed in a ZM, particularly in those cases where the two movies are taken < 10 minutes apart.

By comparing our results to those presented by Kloos et al. (2018) for MY 31–33, it became clear that the problem was arising from the ZM dataset. The mean preferred ACB opacities as measured using the SHMs showed very little interannual variability during the full five MYs of the mission, consistent with expectations. However, the ZM opacities for MY 34–36 are both higher and more variable than those for MY 31–33.

Upon closer inspection, we realized that the mean preferred opacities in the MY 34–36 ZM dataset are being biased upward by a small number of extreme outliers that were not present in the MY 31–33 observations. Almost all of these outliers were associated with ZMs taken close to local noon, just outside of the required keepout window. This suggests that at least one of the high-cloud model's assumptions is breaking down at low phase angles. Indeed, if we plot ZM opacities as a function of the angle between the Navcam pointing and the solar position vector (Figure 4), we can see that there is a clear upward trend towards low angles.

The most obvious candidate for the broken assumption is the phase function term, P(Θ). Kloos et al. (2016) and Kloos et al. (2018) justified the choice of a flat phase function as being consistent with optically thin terrestrial cirrus clouds for scattering angles near 90°. As the Sun approaches the Navcam FOV, we are observing the clouds at progressively smaller scattering angles. Previously derived phase functions for Martian water ice clouds using Viking (Clancy and Lee, 1991), MGS (Clancy et al. 2003), and MSL (Cooper et al., 2019; Innanen et al. 2021) data as well as models of the phase function of different water ice crystal geometries (Yang and Liou, 1996; Yang et al. 2010) all show significant upward deviations from our flat assumption at scattering angles < 40–70°, consistent with the observed effect in our data.

Before our results can yield useful conclusions, we must account for the deviation from our assumptions. The simplest way to do so would be to restrict the dataset to only those where the phase function is flat, throwing out potentially a third to half of the ZM measurements, depending on where we make the cut. Losing such a substantial number of observations would be less than ideal, so it would be preferable to find a way to correct our results, allowing for the use of the entire dataset.

In principle, it would be possible for this correction to be performed using a previously derived phase function for Martian water-ice clouds. However, we are presented with an opportunity to derive our own phase function. Because of the low interannual variability of the ACB, we can assume a constant "true" value for its opacity (after considering seasonal and diurnal effects) and determine what value of the phase function is necessary to bring the calculated opacity down to that value.

In addition to providing another point of comparison, the phase function that we will derive is also fundamentally different methodologically from those reported by Cooper et al. (2019) and Innanen et al. (2021). Because the cloud opacity appears in their phase function equation (a rearranged version of the high-cloud formula), they must use time-averaged water ice column opacities taken by the Mars Climate

Sounder in the vicinity of Gale Crater, which are not necessarily representative of local conditions.

Effects of the MY 34 GDS. Our updated coverage includes the global dust storm (GDS) that occurred in MY 34 between L_s = 188° – 250° (Guzewich et al., 2019). Previous works have found that the ACB in the MY immediately following a GDS can be significantly more variable than those not preceded by a GDS (Mateshvili et al. 2019; Wolff et al. 2019). Although the extremely high atmospheric opacity prevented cloud observations during the storm itself, it is now possible to see if ground-based observations of the ACB following the MY 34 GDS are consistent with these prior observations.

If the MY 34 GDS did impact the opacity of the MY 35 ACB, then that could be problematic for our phase function calculation, as it assumes low interannual variability. However, we do not anticipate this to be a serious problem. It is our expectation that such an effect would expose itself both through the opacities measured at high scattering angles where the assumption of a flat phase function holds as well as through changes in the shape of the derived phase function at low scattering angles, as the phase function itself appears to be unaffected by GDS events (Innanen et al., 2021).

Summary:

The record of cloud opacities over Gale Crater as measured by MSL has been extended from two Martian years to five, covering nearly the entire length of the mission to date (sols 0–3360). We are now able to fully assess interannual variability in diurnal opacity patterns, as well as the effects of the MY 34 GDS on the ACB. In doing so, we found a dependence of the calculated opacities on the scattering angle that is inconsistent with our prior assumption of a flat phase function. In correcting for this dependence, we have an opportunity to derive a phase function for Martian water-ice clouds that is independent of other data sets.

As of writing, the work to derive the phase function and correct the opacity measurements is ongoing. By the time of the conference, we anticipate that we will have a fully corrected record of cloud opacities over Gale Crater through the MY 36 ACB season.

Acknowledgements:

Funding for this research was provided by the Canadian Space Agency MSL Participating Scientist Program based on a NASA MSL PSP selection.

References:

Campbell C.L., Kling A.M., Guzewich S.D., et al. (2020). Estimating the altitudes of Martian water-ice clouds above the Mars Science Laboratory rover landing site. *Planetary and Space Science*, 182(1), 104785.

Clancy R.T., & Lee S.W. (1991). A new look at dust and clouds in the Mars atmosphere: Analysis of emission-phase-function sequences from global Viking IRTM observations. *Icarus*, 93(1). 135-58.

Clancy R.T., Wolff M.J, & Christensen P.R. (2003). Mars Aerosol Studies with the MGS TES emission phase function observations: Optical depths, particle sizes, and ice cloud types versus latitude and solar longitude. *Journal of Geophysical Research*, 108(9).

Cooper B.A., Moores J.E., Ellison D.J., et al. (2019). Constraints on Mars Aphelion Cloud Belt phase function and ice crystal geometries. *Planetary and Space Science,* 168(1), 62–72.

Guzewich S.D., Lemmon M., Smith C.L., et al. (2019). Mars Science Laboratory observations of the 2018/Mars year 34 global dust storm. *Geophysical Research Letters,* 46, 71–79.

Hale A.S., Tamppari L.K., Bass D.S., et al. (2011). Martian water ice clouds: A view from Mars Global Surveyor Thermal Emission Spectrometer. *Journal of Geophysical Research: Planets*, 116(4).

Innanen A.C., Cooper B.A., Campbell C.L., et al. (2021). A comparison of aphelion cloud belt phase functions before and after the Mars year 34 global dust storm. *European Planetary Science Congress 2021*, online, 13–24 Sep 2021, EPSC2021–372.

Kloos J.L., Moores, J.E., Lemmon M., et al. (2016). The first Martian year of cloud activity from Mars Science Laboratory (sol 0–800). *Advances in Space Research*, 57(5), 1223–1240.

Kloos J.L., Moores J.E., Whiteway J.A., et al. (2018). Interannual and Diurnal Variability in Water Ice Clouds Observed from MSL Over Two Martian Years. *Journal of Geophysical Research: Planets*, 123(1), 233–245.

Liu J., Richardson M.I., & Wilson R.J. (2003) An assessment of the global, seasonal, and interannual spacecraft record of Martian climate in the thermal infrared. *Journal of Geophysical Research: Planets*, 108(8), 5089.

Mateshvili N., Fussen D., Vanhellemont F., et al. (2009). Water ice clouds in the Martian atmosphere: Two Martian years of SPICAM nadir UV measurements. *Planetary and Space Science*, 57(8), 1022–2031.

Moores J.E., Lemmon M.T., Rafkin S.C., et al. (2015). Atmospheric movies acquired at the Mars Science Laboratory landing site: Cloud morphology, frequency and significance to the Gale Crater water cycle and Phoenix mission results. *Advances in Space Research*, 55(9), 2217– 2238.

Smith M.D. (2004). Interannual variability in TES atmospheric observations of Mars during 1999–2003. *Icarus*, 167(1), 148–165.

Tamppari L.K, Zurek R.W., & Paige D.A. (2003). Viking-era diurnal water-ice clouds. *Journal of Geophysical Research: Planets*, 108(7), 5073.

Wolff M.J., Bell J.F., James P.B., et al. (1999). Hubble Space Telescope observations of the Martian aphelion cloud belt prior to the Pathfinder mission: Seasonal and interannual variations. *Journal of Geophysical Research: Planets,* 104(4), 9027–9041.

Yang P., & Lieu K.N. (1996). Geometric-optics–integral-equation method for light scattering by nonspherical ice crystals. *Applied Optics*, 35(33), 6568.

Yang P., Gang Hong, Dessler A.E., et al. (2010). Contrails and induced cirrus. *Bulletin of the American Meteorological Society*, 91(4), 473–478.